Research Article | Vol. 26, No. 8 | 16 Apr 2018 | OPTICS EXPRESS 9666
Optics EXPRESS

HCN ppt-level detection based on a QEPAS sensor with amplified laser and a miniaturized 3D-printed photoacoustic detection channel

YING HE,[1] YUFEI MA,[1,*] YAO TONG,[1] XIN YU,[1] AND FRANK K. TITTEL[2]

[1]*National Key Laboratory of Science and Technology on Tunable Laser, Harbin Institute of Technology, Harbin 150001, China*
[2]*Department of Electrical and Computer Engineering, Rice University, 6100 Main Street, Houston, Texas 77005, USA*
**mayufei@hit.edu.cn*

Abstract: Ultra-high sensitive and stable detection of hydrogen cyanide (HCN) based on a quartz-enhanced photoacoustic spectroscopy (QEPAS) sensor was realized using an erbium-doped fiber amplifier (EDFA) as well as a miniaturized 3D-printed photoacoustic detection channel (PADC) for the first time. A HCN molecule absorption line located at 6536.46 cm^{-1} was selected which was in the range of the EDFA emission spectrum. The detection sensitivity of the reported EDFA-QEPAS sensor was enhanced significantly due to the high available EDFA excitation laser power. A 3D printing technique was used to develop the compact PADC, resulting in a size of 29 × 15 × 8 mm^3 and a mass of ~5 g in order to improve the sensor stability and implement sensor applications requiring a compact size and light weight. At atmospheric pressure, room temperature and a 1 s acquisition time, a minimum detection limit (MDL) of 29 parts per billion (ppb) was achieved, corresponding to a normalized noise equivalent absorption (NNEA) coefficient of 1.08×10^{-8} $cm^{-1}W/Hz^{-1/2}$. The long-term performance and the stability of the HCN EDFA-QEPAS sensor system were investigated using an Allan deviation analysis. It indicated that the MDL can be improved to 220 parts per trillion (ppt) with an integration time of 300 s, which demonstrated this compact, integrated and miniaturized 3D-printed PADC based sensor had an excellent stability.

OCIS codes: (280.3420) Laser sensors; (300.6260) Spectroscopy, diode lasers; (280.4788) Optical sensing and sensors.

References and links

1. NIOSH Pocket Guide to Chemical Hazards, "Hydrogen cyanide," https://www.cdc.gov/niosh/npg/npgd0333.
2. T. L. Blank, M. V. Roloff, R. D. Short, S. M. Schuengel, and W. E. Ribelin, "Inhalation toxicity studies of hydrogen cyanide (HCN) in spbague-dawley rats," Toxicol. Lett. **18**, 136 (1983).
3. K. S. Brown and R. R. Robinette, "No simple pattern of inheritance in ability to smell solutions of cyanide," Nature **215**(5099), 406–408 (1967).
4. A. C. Allison, "268. Cyanide-smelling deficiency among africans," Man (Lond.) **53**, 176–177 (1953).
5. W. Carroll, W. Lenney, T. Wang, P. Španěl, A. Alcock, and D. Smith, "Detection of volatile compounds emitted by Pseudomonas aeruginosa using selected ion flow tube mass spectrometry," Pediatr. Pulmonol. **39**(5), 452–456 (2005).
6. L. Dong, A. A. Kosterev, D. Thomazy, and F. K. Tittel, "Compact portable QEPAS multi-gas sensor," Proc. SPIE **7945**, 79450R (2011).
7. A. A. Kosterev, F. K. Tittel, and G. Bearman, "Advanced quartz-enhanced photoacoustic trace gas sensor for early fire detection," SAE Int. J. Aerosp. **1**(1), 331–336 (2008).
8. E. Lellouch, M. Gurwell, B. Butler, T. Fouchet, P. Lavvas, D. F. Strobel, B. Sicardy, A. Moullet, R. Moreno, D. Bockelée-Morvan, N. Biver, L. Young, D. Lis, J. Stansberry, A. Stern, H. Weaver, E. Young, X. Zhu, and J. Boissier, "Detection of CO and HCN in Pluto's atmosphere with ALMA," Icarus **286**, 289–307 (2017).
9. S. F. Rastegar, A. A. Peyghan, and N. L. Hadipour, "Response of Si-and Al-doped graphenes toward HCN: a computational study," Appl. Surf. Sci. **265**, 412–417 (2013).
10. M. T. Baei, "$B_{12}N_{12}$ sodalite like cage as potential sensor for hydrogen cyanide," Comput. Theor. Chem. **1024**, 28–33 (2013).

#321001 https://doi.org/10.1364/OE.26.009666
Journal © 2018 Received 30 Jan 2018; revised 26 Mar 2018; accepted 30 Mar 2018; published 4 Apr 2018

Optics EXPRESS

11. R. Gotor, A. M. Costero, S. Gil, M. Parra, R. Martínez-Máñez, F. Sancenón, and P. Gaviña, "Selective and sensitive chromogenic detection of cyanide and HCN in solution and in gas phase," Chem. Commun. (Camb.) **49**(50), 5669–5671 (2013).
12. R. K. Lauridsen, T. Rindzevicius, S. Molin, H. K. Johansen, R. W. Berg, T. S. Alstrøm, K. Almdal, F. Larsen, M. S. Schmidt, and A. Boisen, "Towards quantitative SERS detection of hydrogen cyanide at ppb level for human breath analysis," Sens. Bio-Sensing Res. **5**, 84–89 (2015).
13. D. Marchenko, A. H. Neerincx, J. Mandon, J. Zhang, M. Boerkamp, J. Mink, S. M. Cristescu, S. Te Lintel Hekkert, and F. J. M. Harren, "A compact laser-based spectrometer for detection of C_2H_2 in exhaled breath and HCN in vitro," Appl. Phys. B **118**(2), 275–280 (2015).
14. K. R. German and W. S. Gornall, "Photoacoustic spectroscopy of the v3 band of HCN," J. Opt. Soc. Am. **71**(21), 1452–1457 (1981).
15. A. A. Kosterev, Y. A. Bakhirkin, R. F. Curl, and F. K. Tittel, "Quartz-enhanced photoacoustic spectroscopy," Opt. Lett. **27**(21), 1902–1904 (2002).
16. Y. F. Ma, Y. He, X. Yu, J. B. Zhang, R. Sun, and F. K. Tittel, "Compact all-fiber quartz-enhanced photoacoustic spectroscopy sensor with a 30.72 kHz quartz tuning fork and spatially resolved trace gas detection," Appl. Phys. Lett. **108**(9), 091115 (2016).
17. H. M. Yi, R. Maamary, X. M. Gao, M. W. Sigrist, E. Fertein, and W. D. Chen, "Short-lived species detection of nitrous acid by external-cavity quantum cascade laser based quartz-enhanced photoacoustic absorption spectroscopy," Appl. Phys. Lett. **106**(10), 101109 (2015).
18. M. Mordmueller, W. Schade, and U. Willer, "QEPAS with electrical co excitation for photoacoustic measurements in fluctuating background gases," Appl. Phys. B **123**(8), 224 (2017).
19. S. Borri, P. Patimisco, I. Galli, D. Mazzotti, G. Giusfredi, N. Akikusa, M. Yamanishi, G. Scamarcio, P. De Natale, and V. Spagnolo, "Intracavity quartz-enhanced photoacoustic sensor," Appl. Phys. Lett. **104**(9), 091114 (2014).
20. H. Zheng, L. Dong, Y. Ma, H. Wu, X. Liu, X. Yin, L. Zhang, W. Ma, W. Yin, L. Xiao, and S. Jia, "Scattered light modulation cancellation method for sub-ppb-level NO_2 detection in a LD-excited QEPAS system," Opt. Express **24**(10), A752–A761 (2016).
21. Y. He, Y. F. Ma, Y. Tong, X. Yu, Z. F. Peng, J. Gao, and F. K. Tittel, "Long distance, distributed gas sensing based on micro-nano fiber evanescent wave quartz-enhanced photoacoustic spectroscopy," Appl. Phys. Lett. **111**(24), 241102 (2017).
22. K. Liu, W. X. Zhao, L. Wang, T. Tan, G. S. Wang, W. J. Zhang, X. M. Gao, and W. D. Chen, "Quartz-ehanced photoacoustic spectroscopy of HCN from 6433 to 6613 cm^{-1}," Opt. Commun. **340**, 126–130 (2015).
23. A. A. Kosterev, F. K. Tittel, D. V. Serebryakov, A. L. Malinovsky, and I. V. Morozov, "Applications of quartz tuning forks in spectroscopic gas sensing," Rev. Sci. Instrum. **76**(4), 043105 (2005).
24. Z. Wang, Z. Li, and W. Ren, "Quartz-enhanced photoacoustic detection of ethylene using a 10.5 μm quantum cascade laser," Opt. Express **24**(4), 4143–4154 (2016).
25. Y. Ma, R. Lewicki, M. Razeghi, and F. K. Tittel, "QEPAS based ppb-level detection of CO and N_2O using a high power CW DFB-QCL," Opt. Express **21**(1), 1008–1019 (2013).
26. J. P. Waclawek, H. Moser, and B. Lendl, "Compact quantum cascade laser based quartz-enhanced photoacoustic spectroscopy sensor system for detection of carbon disulfide," Opt. Express **24**(6), 6559–6571 (2016).
27. Y. Ma, G. Yu, J. Zhang, X. Yu, R. Sun, and F. K. Tittel, "Quartz enhanced photoacoustic spectroscopy based trace gas sensors using different quartz tuning forks," Sensors (Basel) **15**(4), 7596–7604 (2015).

1. Introduction

Hydrogen cyanide (HCN) is a colorless and extremely poisonous gas molecule. It is usually released in industrial processing and is an important precursor to many chemical compounds. Exposure to HCN of < 4.7 ppm, as recommended by the National Institute for Occupational Safety and Health, NIOSH, is the maximum safe exposure concentration level, because HCN inhibits the consumption of oxygen by biological cells [1,2]. Due to genetic characteristics, not all people are able to perceive the almond-like odor of HCN [3,4]. Furthermore, HCN was identified as a biomarker in the breath of cystic fibrosis (CF) patients [5]. HCN is also generated by the incomplete combustion of nitrogen-containing polymers, such as plastics, polyurethanes and paper. Therefore, HCN detection is important in early fire detection warning on board of aircraft or spacecraft [6,7]. In addition, the presence of HCN has also observed in planetary atmospheric environmental exploration [8].

In recent years, several techniques for HCN detection have been investigated. An electrochemical sensor uses doped graphene and other electronic materials as a key component which changes the conductance after exposure to HCN gas with merits of compactness and low cost. However, electrochemical sensors are constrained due to poor detection limits and a long response time [9,10]. Colorimetric chemical sensors are of special

Optics EXPRESS

interest because of their low cost and selectivity. But such sensors have the shortcomings of limited detection limits, long response time and temporal degradation [11]. Sensor platforms based on laser spectroscopy such as surface-enhanced Raman spectroscopy (SERS), tunable diode laser absorption spectroscopy (TDLAS) and photoacoustic spectroscopy (PAS) can be used for HCN gas detection. These sensors typically achieve a detection limit of ppm or ppb HCN concentration levels [12–14].

An innovation of microphone-based photoacoustic spectroscopy (PAS), namely quartz-enhanced photoacoustic spectroscopy (QEPAS) was first reported in 2002 [15]. The QEPAS technique utilizes a tiny piezoelectric quartz tuning fork (QTF) as the sensing element to detect the acoustic wave which is generated by the targeted gas analyte as a result of light absorption. The standard QTF is commercially available, inexpensive, millimeter sized with a high Q-factor (~10,000 at 1 atm and~100,000 in vacuum) and a narrow resonance frequency band, which results in excellent immunity to environmental noise [16]. In comparison to a SERS gas sensor, the QEPAS-based sensor does not need to sample the gas analyte and therefore can maintain online detection. Furthermore, the QEPAS-based sensor is compact compared to TDLAS, since the photoacoustic signal is not proportional to the length of absorption path. Therefore, with its merits of high sensitivity, fast response and compactness, the QEPAS based gas sensor is an excellent method for trace gases detection [17–21].

In this paper, an ultra-high sensitive detection of HCN based on an erbium-doped fiber amplifier (EDFA) amplified QEPAS sensor with a miniaturized 3D-printed photoacoustic detection channel (PADC) is reported for the first time. With the use of a 3D-printed PADC, the optical and photoacoustic detection components of the reported sensor are more compact and reliable in contrast to a conventional QEPAS system. An EDFA with a maximum output power of 1200 mW was utilized to amplify the diode laser output power. A QTF with low resonance frequency of 30.72 kHz was utilized as the acoustic wave transducer. The performance of gas sensor was investigated and optimized, which resulted in a ppt-level HCN detection sensitivity. Further potential performance improvements for the current sensor are also discussed.

2. Experimental setup

2.1 Selection of HCN absorption line

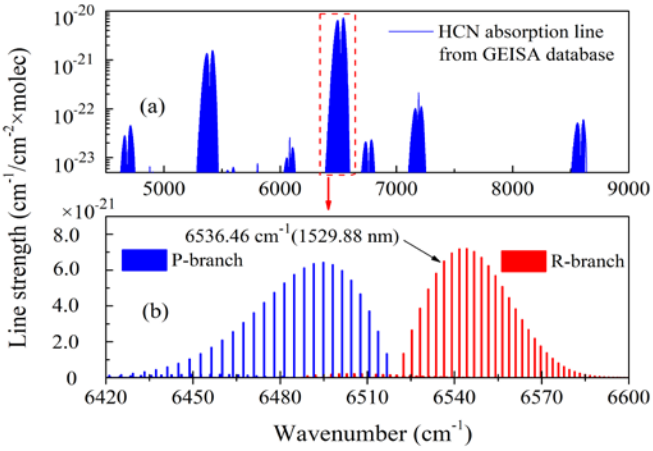

Fig. 1. The calculated near infrared (NIR) HCN absorption line based on the GEISA database: (a) the absorption line in the NIR range; (b) line strength within the 6420-6600 cm^{-1} spectral range

The calculated near infrared (NIR) HCN absorption line strength based on the GEISA database is shown in Fig. 1. The strongest HCN absorption region is located in the 6420-6600

Optics EXPRESS

cm^{-1} spectral range, corresponding to a commercial optical communications band, which has many available cost-effective laser sources. Figure 1(b) illustrates the HCN molecular absorption line strength within the 6420-6600 cm^{-1} spectral range, which covers both the R and P branches [22]. In this experiment, a strong absorption line of 6536.46 cm^{-1} (1529.88 nm) in the R-branch was selected, which is free from spectral interference of other gas species.

In a QEPAS based sensor system, the signal amplitude S is governed by the following equation [23]:

$$S \propto \frac{\alpha PQ}{f_0} \tag{1}$$

where α is the absorption coefficient, P is the optical excitation power, Q is the Q-factor of QTF and f_0 is the QTF resonance frequency. Since the signal amplitude varies linearly with the optical excitation power, the performance of the QEPAS sensor can be improved by increasing the excitation laser power. This property differs from other spectra based sensor such as SERS and TDLAS [12,13]. Diode lasers are usually used in QEPAS technique because of their compactness and narrow line width. However, the laser output power is in the milliwatt range, which limits the QEPAS sensing performance. Optical fiber amplifiers, which are widely used in optical communications (with three operating wavelength bands, S band: 1450-1550 nm, C band: 1520-1570 nm, and L band: 1565-1610 nm) can be employed to provide a significant optical signal amplification. Therefore, a commercial erbium-doped fiber amplifier (EDFA) was implemented to enhance the diode laser output power. To minimize the dominant amplified spontaneous emission (ASE) noise in an EDFA, a narrow-band filter with a bandwidth of 1.2 nm and a center wavelength of 1530.33 nm was utilized, which resulted in an output spectrum of ~1529.73-1530.93 nm. The selected absorption line of 1529.88 nm is in the range of EDFA.

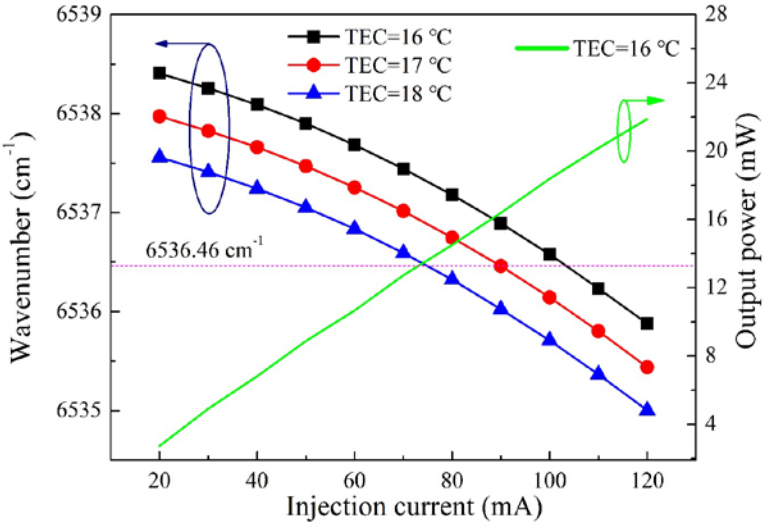

Fig. 2. 1.53 μm CW-DFB diode laser output performance as function of injection current and at three operating temperatures of the laser thermoelectric cooler (TEC)

The diode laser output performance was investigated and is shown in Fig. 2. The experimental determined temperature and current tuning coefficients of the laser were –0.43 cm^{-1}/cm^{-1} and –0.025 cm^{-1}/mA, respectively. The maximum optical power emitted by the diode laser operating at a temperature of 16 °C and an injection current of 120 mA was 22 mW. Therefore, the diode laser can be tuned to target the HCN absorption line of 6536.46

Optics EXPRESS

cm^{-1} by setting the TEC operating temperature of diode laser at 16 °C to obtain the highest output power.

2.2 3D-printed photoacoustic detection channel

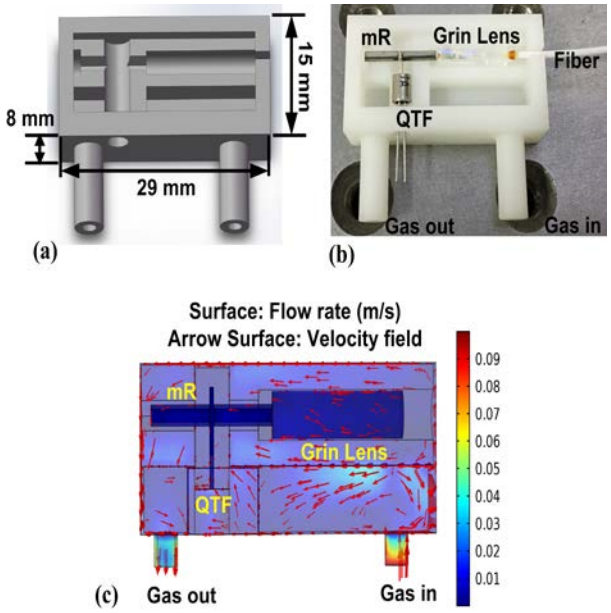

Fig. 3. The 3D-printed PADC: (a) A designed 3D model; (b) 3D-printed PADC including a grin lens, a QTF and mRs; (c) the flow field within the PADC

In a traditional QEPAS system, the excitation laser is delivered to the PADC by a group of lenses [24–26]. As a result, the large size and unstable optical configuration from discrete components limits the sensor's performance and practical applications. The 3D printing technique with the advantages of high integration and stability provides an ease of fabrication. In this research, the PADC was made by a 3D laser printing technique which used an UV-curable resin as the processing material. Figure 3 shows the design of PADC, the fabricated product as well as the assembled optical and photoacoustic detection components, and the flow field within the PADC simulated by COMSOL Multiphysics software. The 3D-printed PADC has a length of 29 mm, a width of 15 mm and a thickness of 8 mm. With an internal volume of 1.5 cm^3, the assembled gas chamber of the 3D-printed PADC was sealed by a quartz glass window with UV-curing glue. The laser was transmitted and focused by a fiber-connected grin lens with a diameter of 1.8 mm. Beyond the grin lens, there was a QTF as well as a pair of micro-resonators (mRs) with a 25 μm gap. The laser beam could pass through the QTF prongs and the mR without touching. The remainder of the laser power was transmitted out of the PADC through a quartz glass window behind the mRs. All the components were assembled together and the total weight of the 3D-printed PADC including the grin lens, QTF and mRs was ~5 g.

2.3 Experimental setup

The experimental configuration of HCN detection sensor system is depicted in Fig. 4. Wavelength modulation spectroscopy (WMS) with 2nd harmonic detection was employed for sensitive HCN concentration measurements. Modulation of the laser current was controlled by applying a sinusoidal dither to the direct current ramp at the half of the QTF resonance frequency (f_0). A 1.53 μm continuous wave, distributed feedback (CW-DFB) fiber-coupled diode laser was used as the laser excitation source. The diode laser output was amplified by

Optics EXPRESS

an EDFA with two-stage amplifier and was delivered to the 3D-printed PADC via a grin lens. Inside the 3D-printed PADC, the HCN molecules were stimulated by the excitation laser in order to generate an acoustic wave at a frequency, which was equal to twice the laser modulation frequency. The acoustic wave between QTF prongs was accumulated and amplified by a pair of mRs, so that the piezoelectric signal generated by the QTF was enhanced. Subsequently, a low-noise transimpedance amplifier (TA) with a 10 MΩ feedback resistor and a lock-in amplifier were employed to increase and demodulate the piezoelectric signal into a 2*f* signal (namely the QEPAS signal). The data acquired by the sensor system was processed by a computer (PC) using LabVIEW software. A mass flow controller with an uncertainty of 3% was used to dilute a 50 ppm HCN:N_2 mixture and to control the flow rate at 120 mL/min. The sensor was operated at atmospheric pressure and room temperature.

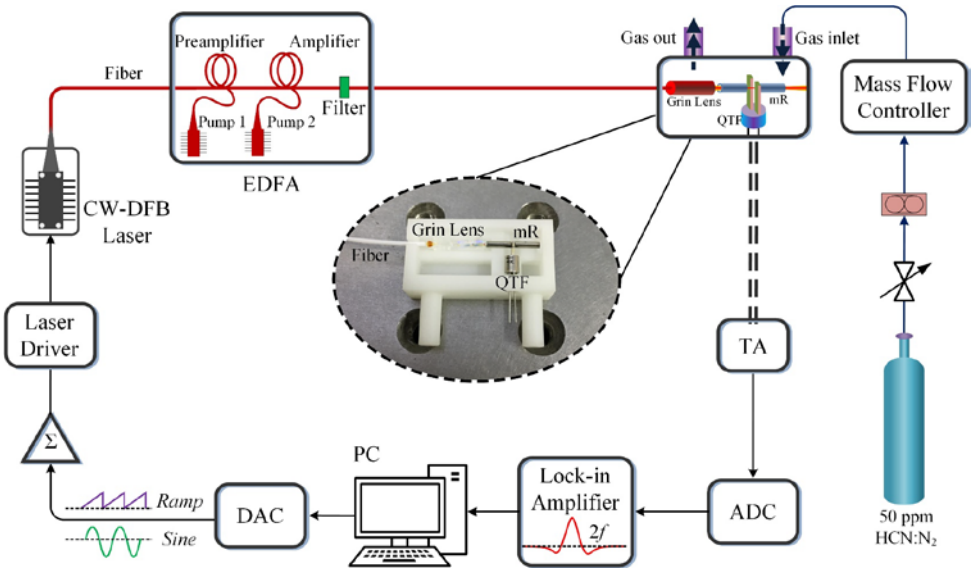

Fig. 4. Schematic of the EDFA-QEPAS sensor system for HCN detection

3. Results and Discussion

In the reported research, a QTF with a f_0 of 30.72 kHz was used. According to Eq. (1), a QTF with lower resonance frequency is advantageous in order to obtain a larger QEPAS signal [27]. Therefore, the advantage of the QTF with f_0 of 30.72 kHz was compared to a standard 32.768 kHz QTF. The experiments were performed for the same conditions and the results are shown in Fig. 5. It can be seen that the 2*f* amplitude signal increased 1.2 times when a QTF with a f_0 of 30.72 kHz was employed compared to that of a 32.768 kHz QTF. Two parameters contribute to an increase of the QEPAS signal. One parameter is the lower resonance frequency f_0. The other is Q-factor of QTF which was measured experimentally. The Q-factors for QTF with a f_0 of 32.768 kHz and 30.72 kHz were 5,546 and 6,267, respectively.

Optics EXPRESS

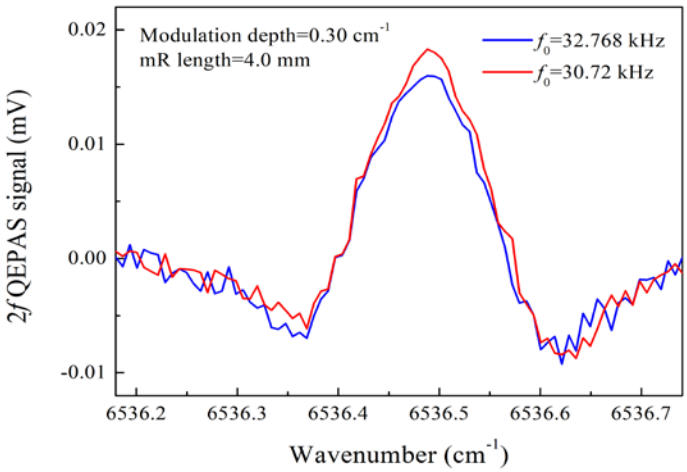

Fig. 5. 2*f* signal for two QTFs with different f_0 values of 30.72 kHz and 32.768 kHz at the same experimental conditions

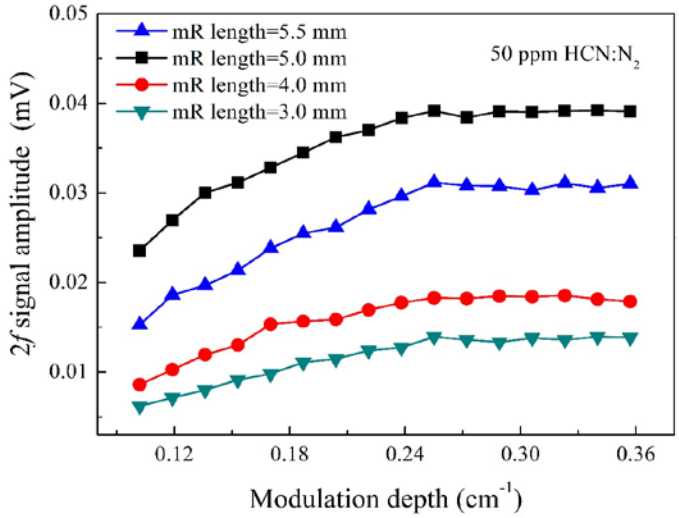

Fig. 6. 2f signal amplitude with different mRs as a function of modulation depth

A significant improvement of the QEPAS signal can be obtained when a pair of metallic tubes acting as a micro-resonator (mR) is included in the QTF sensor architecture. The optimum length of mR tubes should be in the range of $\lambda_s/4$~$\lambda_s/2$, where λ_s is the sound wavelength. Hence a range of 2.8~5.5 mm is the optimum length of mR tubes with a sound velocity of 340 m/s and a frequency of 30.72 kHz. In this experiment, the inner diameter of stainless tube was chosen to be 0.5 mm and different lengths of 3.0, 4.0, 5.0 and 5.5 mm were investigated, respectively. The measured 2*f* signal amplitude with different mRs as a function of the laser wavelength modulation depth is illustrated in Fig. 6. From Fig. 6, it can be seen that the maximum signal was achieved when two mR tubes with a length of 5.0 mm were utilized. Furthermore, the 2*f* signal amplitude increased when the modulation depth increased and it did not change appreciably when the modulation depth was >0.26 cm^{-1}. Therefore, the mR tubes with a length of 5 mm and a laser wavelength modulation depth of 0.26 cm^{-1} were employed in the following investigation.

Optics EXPRESS

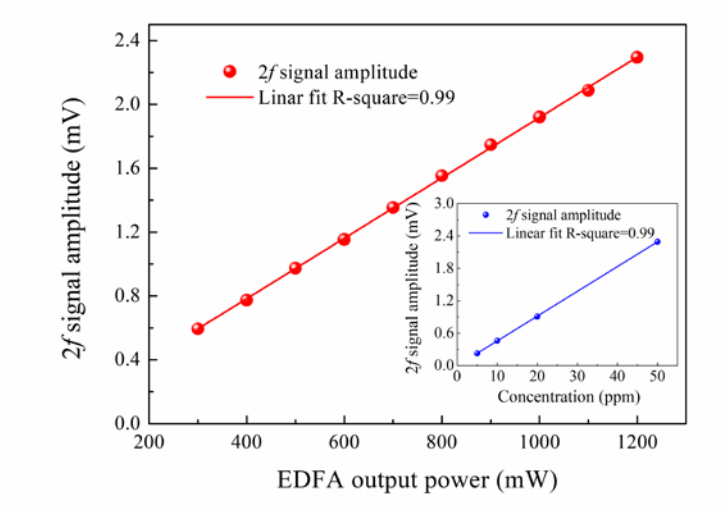

Fig. 7. EDFA-QEPAS 2*f* signal amplitude as a function of optical power at a modulation depth of 0.26 cm^{-1}. Insert for the 2*f* signal amplitude as a function of HCN concentrations

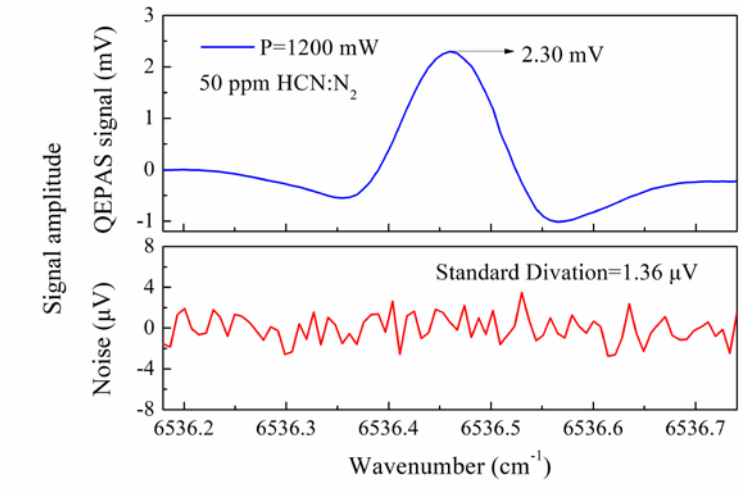

Fig. 8. 2*f* signal with EDFA amplified output power of 1200 mW and the background noise with pure N_2

To improve the sensitivity of HCN detection system, the EDFA-QEPAS sensor performance was investigated when the optical output power of amplified diode laser was varied from 300 to 1200 mW. The measured 2*f* signal amplitude as a function of the EDFA output power and the HCN concentrations (5-50 ppm) is depicted in Fig. 7. The amplitude of the 2*f* signal improved with increasing EDFA amplified output power and the concentration. The calculated R-square value of a linear fit of the 2*f* signal for both is equal to ~0.99, which indicates that the reported HCN sensor exhibits an excellent linearity response of the excitation laser power levels as well as the HCN concentrations. Saturable absorption effects did not occur, which means that the EDFA-QEPAS performance can be further improved when an EDFA with an even higher amplified power output is adopted. Figure 8 depicts the 2*f* signal when an EDFA output power of 1200 mW and an HCN concentration of 50 ppm were used. The background signal was measured when the 3D-printed PADC was filled with pure N_2. Based on the data depicted in Fig. 8, the 1σ minimum detection limit (MDL) of the

Optics EXPRESS

HCN EDFA-QEPAS sensor was 29.6 ppb for a 1 s time constant of the lock-in amplifier. The corresponding normalized noise equivalent absorption (NNEA) coefficient is 1.08×10^{-8} $cm^{-1}W/Hz^{-1/2}$, which was calculated from the following equation: NNEA = $(\alpha_{min} \cdot P)/\sqrt{\Delta f}$, where α_{min} is the minimum detectable absorption coefficient for SNR = 1, P is the optical power and $\sqrt{\Delta f}$ is the detection bandwidth.

To assess the long-term stability of EDFA-QEPAS sensor based HCN detection, an Allan deviation analysis was performed. The 3D-printed PADC was filled with pure N_2 and the measurement lasted for more than two hours. The result is shown in Fig. 9, which implies that a MDL of 220 ppt was achieved when the integration time for the HCN-QEPAS sensor with a 3D-printed PADC is 300 s. The MDL improvement was two orders of magnitude and demonstrated that this compact and miniaturized 3D-printed PADC based sensor has an excellent stability.

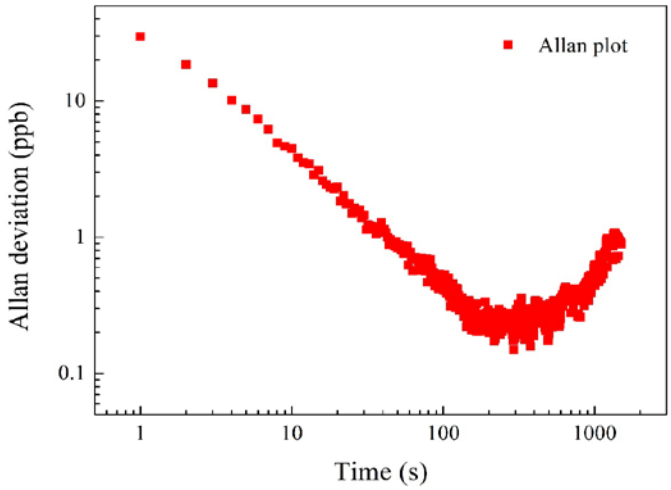

Fig. 9. Allan deviation analysis for time series measurements of pure N_2

4. Conclusions

In conclusion, an ultra-high sensitive EDFA-QEPAS sensor with a miniaturized 3D-printed PADC for HCN detection was demonstrated. An EDFA with an amplified output power of 1200 mW was employed to enhance the detection sensitivity of the reported HCN sensor. Furthermore, a 3D-printed PADC was developed in order to improve the sensor stability and be useful in real world applications of such a HCN sensor system. The detection channel is a compact device containing optical and photoacoustic detection components with a dimension of $29 \times 15 \times 8$ mm^3 as well as a mass of the whole structure of ~5 g. A QTF with a resonance frequency of 30.72 kHz was utilized as the acoustic wave transducer. After optimizing the laser wavelength modulation depth and the length of the mR tubes, a MDL of 29 ppb for HCN detection was obtained with a 1 s integration time and an EDFA amplified output power of 1200 mW, which corresponds to a NNEA of 1.08×10^{-8} $W \cdot cm^{-1} \cdot Hz^{-1/2}$. With an integration time of 300 s, the MDL was significantly improved to be 220 ppt and demonstrated that this compact, integrated and miniaturized 3D-printed PADC based sensor is capable of excellent stability. In addition, since no saturable absorption effects were observed with a 1200 mW excitation laser applied, the sensor's capability can be further improved when an EDFA with a higher amplified output power and an optimized humidity condition are implemented.

Optics EXPRESS

Funding

The National Natural Science Foundation of China (61505041); the Natural Science Foundation of Heilongjiang Province of China (F2015011); the Financial Grant from the China Postdoctoral Science Foundation (2014M560262 and 2015T80350); the Financial Grant from the Heilongjiang Province Postdoctoral Foundation (LBH-Z14074 and LBH-TZ0602); the Fundamental Research Funds for the Central Universities, the Application Technology Research and Development Projects of Harbin (2016RAQXJ140); the US National Science Foundation ERC MIRTHE award and the Welch Foundation (C-4925U).